Research Square

Preprints are preliminary reports that have not undergone peer review.
They should not be considered conclusive, used to inform clinical practice,
or referenced by the media as validated information.

Pressure Induced Changes in Grain Boundary Conditions of Lithium Conducting Ceramics Characterized by Impedance Spectroscopy

John W. Ostrander (john.ostrander@gmail.com)
University of Tulsa Dept. of Chemistry and Biochemistry https://orcid.org/0000-0002-0268-224X
Carolyn Torres
University of Tulsa Dept. of Chemistry and Biochemistry
Fride Vullum-Breuer
Norwegian University of Science and Technology
Dale Teeters
University of Tulsa Dept. of Chemistry and Biochemistry

Research Article

Keywords: Pressure, Grain Boundary Conditions, Lithium Conducting Ceramics, Impedance Spectroscopy, Solid state batteries, lithium ion

Posted Date: June 25th, 2021

DOI: https://doi.org/10.21203/rs.3.rs-646054/v1

License: This work is licensed under a Creative Commons Attribution 4.0 International License.
Read Full License

Pressure Induced Changes in Grain Boundary Conditions of Lithium Conducting Ceramics Characterized by Impedance Spectroscopy

John W. Ostrander*[1], Carolyn Torres[1], Fride Vullum-Breuer[2], and Dale Teeters[1]

1. University of Tulsa Dept. of Chemistry and Biochemistry, 800 South Tucker Tulsa OK 74104
2. Norwegian University of Science and Technology, Dept. of Materials Science and Engineering, Trondheim Norway
*Corresponding author email john.ostrander@gmail.com; Dale Teeters; dale-teeters@utulsa.edu; Fride Vullum-Breuer, fride.vullum.bruer@sintef.no; Carolyn Torres, cdb524@utulsa.edu

Abstract

Solid state batteries, particularly for lithium ion based architecture have been the focus of development for over 20 years and are receiving even more attention today. Utilizing impedance spectroscopy (IS) measurements we investigate the response of conductivity versus incremental pressure increase by a piston-cylinder-type high pressure cell up to 1 GPa for some lithium conducting ceramics: LATP ($Li_{1.3}Al_{0.3}Ti_{1.7}(PO_4)_3$), LLTO ($Li_5La_3Ta_2O_{12}$), LLT ($Li_{0.33}La_{0.55}TiO_3$), LAGP ($Li_{1.5}Al_{0.5}Ge_{1.5}P_3O_{12}$) and LLZO ($Li_7La_3Zr_2O_{12}$) for non-annealed and annealed samples.

Isothermal, incremental pressure increase of powders allows for an *in situ* observation of the transition state conditions of poorly consolidated ceramic powders and the effects on grain boundary conditions prior to sintering. Specific conductance (σ_b) increased by several orders of magnitude in some samples, approaching 10^{-3} $S \cdot cm^{-1}$, yet decreased in other samples. The affect of grain boundaries and affects of bulk capacitance as the sample dimensions are altered due to pressure, are attributed to some of this behavior and will be discussed. The understanding of some of these fundamental processes may be valuable in facilitating these and similar ceramics for use in commercial solid state battery systems.

1. Introduction

Lithium ion batteries have been in widespread production and use in personal electronics since the early 1990s. Since then advances have occurred incrementally, with improved performance, higher energy density, and smaller battery size. Batteries that once were quite large are now very condensed, while maintaining the same power and energy storage as much larger cells. This is desirable for lightweight portable electronics, but with the side effect of improved performance these much smaller batteries are doing the same amount of work as their larger fore-runners and heat evolution is an unavoidable consequence. Battery ignition, fires, and explosions of

lithium cells has resulted in many changes in policy, regulations, and law, notably that free lithium batteries are not permitted in carry on bags with most airlines.

Other considerations are the affects of pressure and the affects on battery degradation under load which would be important with the development of commercial solid state battery systems.

Several solutions have resulted from this problem such as increased interest in the areas of inflammable electrolytes, better battery design, and solid state lithium batteries among others. It is widely stated in publications over the last several years that solid state batteries (SSB) are one solution for problems lithium ion batteries (LIB) such as dendrite formation, over heating, etc. Generally speaking, solid state batteries are as not widely available, and only recently emerging on the commercial market most notably with electric vehicles.

Here, we look at five commercially available lithium containing ceramics as candidates for the solid electrolyte for SSB[1-2]. As a solid state electrolyte, ceramics are better suited for higher temperatures[3,4] which can simultaneously address the issue of safety as well as performance.

Investigated in this work are garnets LLTO ($Li_5La_3Ta_2O_{12}$)[5-8] and LLZO ($Li_7La_3Zr_2O_{12}$)[9], LATP (NASICON[10] structure), LAGP($Li_{1.5}Al_{0.5}Ge_{1.5}P_3O_{12}$), and perovskite LLT ($Li_{0.33}La_{0.55}TiO_3$)[11]. In an effort to reconcile grain boundary conditions and resulting affects on ion conductivity (σ_b), each powder was analyzed by impedance spectroscopy *in situ* to observe changes in grain boundary conditions. The grain boundary phase[12] may be detected separately[8,12], or inclusively[13], but it was not found that *in situ* studies of grain boundaries have been characterized in this way. We should first define the grain boundary as not only the area of grain-grain contact, but also the adjacent regions and voids where grains are in very close proximity without touching. This definition of grain boundaries has been inferred previously in other publications [14-15]. For simplicity this interpretation is used here as these grain boundaries are variable and expected to change (along with sample thickness) under increased pressures.

Identified in 1968[16], LATP belongs to space group R3C[17-18]. Considered a super-ionic conductor[19] and air stable[20], the crystal structure most similar to NASICON ($Na_{1+x}Zr_2Si_xP_{3-x}O_{12}$, $0 < x < 3$)[21] which has been studied intensively since the 1980s for use in sodium or lithium sulfur batteries[18,22]. LATP has also been described as rhombehedral[23]. Ion migration pathways in LATP have been modeled for both sodium[24] and lithium[25,14] so much is already known about the bulk ceramic and single crystal form. LAGP also has a NASICON-like structure[26], sometimes referred to as LISICON[25] and is less studied than LATP. LATP and LAGP are thus promising due to the super ionic conduction and resistance to lithium metal[2,20]. Conversely LATP Lithium reactions have also

been reported[5, 20, 27] leaving the door open to additional characterization. The presence of trivalent metal ions in the structure can improve bulk ion conductance (σ_b) [28-31] but this is not expected to be the case here.

LLZO as received has a garnet structure. When calcined at 1150°C or by other methods[32-33] LLZO recrystalizes to a cubic phase (c-LLZO) [20, 34-35]. The cubic phase is considered a super ion conductor[7], but is less stable than the garnet phase and was not investigated here. Doping of LLZO with aluminum is possible and has been shown to improve conduction[29, 36], but was avoided here with the use of quartz sample boats for heating.

First mentioned in literature in 1993[37], LLTO is considered an exceptional ion conductor[5] that is temperature independent[38]. Because of high grain boundary impedance (Z_{GB}), some say that LLTO is a better insulator than it is an ion conductor[39]. Contrarily, Sakamaki *et al* report that partial grain boundaries have higher current flow, and the high grain boundary resistance can be overcome[40].

Perovskite LLT has been well characterized as a bulk material[11] and having high σ_b, but also dominated by grain boundary resistance even under pressure[41-45]. This reasoning is supported by Inaguma *et al* whom describe elimination of the grain boundary resulting in improved conductance for LLT[46]. On the other hand, LLT is also reported as reactive with lithium metal[46].

If lithium metal could be used for anode material, the energy densities of 3860 $mAhg^{-1}$ and oxidation potential of -3.04V vs. SHE would be a significant step in LIB development, but this has so far been a poor candidate due to high reactivity, and dendrite formation[47]. This includes solid state electrolytes[48] and the solid electrolyte interphase (SEI) formed when using lithium metal anodes.

We hypothesize that by characterizing lithium ion conducting ceramics *in situ* that we can learn more about the grain boundary interactions and perhaps lay the groundwork for future modeling of these and similar systems. By using commercially available materials, we expect there to be more reproducibility and consistency than experimental or synthesized powders which would add more variables to the study. While used as received, powders were also annealed to relieve internal stressors, and cracks, for a more uniform and optimized powder free from such physical defects as much as possible for additional tests for comparison, while heating below temperatures that would effect recrystallization or sintering.

2. Materials and methods

2.1 Materials

Ceramics were used as received from Toshima Ltd. (Japan). For sample testing, a KBr pellet press (international crystal laboratories) with vacuum capability was used without modification. Non-porous alumina tubing and E52100 alloy steel were purchased from McMaster Carr. Impedance spectroscopy was taken with a Solartron 1296 interface and a Solartron 1260 gain phase analyzer. Impedance data was analyzed using Zview®, and any images were processed in ImageJ 1.50i. Helios Nanolab 600, Fe-SEM (Zeiss Ultra 55 LE, and LV-Fe-SEM (Zeiss Supra 55 VP) were used for SEM imaging, and XRD were conducted on Rigaku XRD. Thermogravimetric (TGA) was performed on TA instrument "Discovery" series TGA in platinum pans. Redundant calculations were performed in Microsoft Excel 2007. Battery cycling was performed with a Maccor 4300M in tandem with a Parstat (Princeton technologies) 4000+. Any glovebox work was conducted inside an MBraun glovebox with typical O_2 levels below 5ppm.

2.2 Methods

Annealing of powders was done in a tube furnace in alumina boats (except LLZO to avoid Al doping), under argon at specific temperatures for each ceramic. Annealing time was not less than 4 hours for any sample. Reduction of LATP occurred, resulting in the characteristic blue color which was reversible upon subsequent heating in air. The function of annealing reduces average particle size, as explained by Jackman *et al*[49]:

$$GS_{critical} = \frac{14.4\,\gamma}{E(\Delta\alpha_{max})^2(\Delta T)^2} \qquad (1)$$

γ_f is fracture surface energy, and $\Delta\alpha_{max}$ is the difference in maximum and minimum principal axis of a unit cell, or grain. Annealing was used in an attempt to procure more pristine grains, and perhaps narrower grain size distribution.

Each sample was subjected to pressure in custom test cell for *in situ* impedance testing. It was convenient to use a pellet press, originally made for FTIR salt pellets, with a removable alumina tube cut to size was used as an insulator inside the sample holder. Positioning the sample holder and steel shaft reduced incident of alumina tube breakage, but likewise under such pressures cracking of the alumina tube did not compromise the sample, as powders are not fluid and pelletize when subjected to pressure. The polished anvil, part of the pellet press, served as one electrode surface, which was in contact with the metal pellet press, and The hardened steel shaft served as the other

electrode. The sample holder was set on a blank electronic"bread board" which does not compress, to insulate from the hydraulic press surface.

About 0.2 grams of powder is introduced into the tube. The steel shaft is inserted into the tube, and O-rings were used on both shaft and tube to facilitate vacuum. The hydraulic press was used to apply pressure such that the pressure gauge registered, and was referred to here as 0.00GPa pressure.

The sample powder was tested under a range of pressure from 0.00 to 1.00 GPa, at incremental steps. The pressure forces closer fitting of grains, streamlining the ion migration[50] by closing the grain-grain voids, and forcing more grain-grain surface contact. Alternatively, this conductance may improve simply by increasing the sample density[21]

2.3 Impedance Spectroscopy (IS)

Bulk resistance is derived using equation 2, and the ion conductance by equation 3. It is important to indicate that ion conductivity is an intrinsic quantity characterizing the entire (bulk) sample. *For this particular work the sample thickness, and volume, change with pressure*. Bulk resistance (R_b) is described by equation (2) and bulk conductance (σ or σ_b) by equation (3):

$$\omega R_b C_b = 1 \quad \text{and} \quad R_b = \frac{1}{\omega C_b} \tag{2}$$

$$\sigma = \frac{l}{R_b A}, \text{and } \partial\sigma = \frac{\partial l}{\partial R_b A} \tag{3}$$

In equation 2, ω = angular frequency and C_b= bulk capacitance. Equation 3 has two parts, the convention for conductance at constant conditions, and the change in conductance roughly calculated dependent on a change of sample thickness (∂l), and resistance, ∂R_b. A is electrode surface area in contact with sample, and l is sample thickness.

Determination of sample thickness *in situ* was determined by the difference of the height of the hydraulic press from the top of the sample holder after settling at each pressure increment, and the height of an empty cell with some pressure applied. A feeler gauges and micrometer were used exhaustively in determination of sample thickness.

Impedance spectra were typically taken from 10MHz to 0.075 Hz for each sample, at pressure increments from 0 to 1.00GPA pressure (0.75 GPa was used in some samples, higher pressures were not always sustainable).

Electric modulus is useful for materials characterization[15, 51-55]. Likewise tan δ, and permittivity ε^* ($\varepsilon^* = \varepsilon' - j\,\varepsilon'', j = \sqrt{-1}$) may also be used in this case to characterize the changes in grain boundary conditions and were useful in determining the correct equivalent circuit. Bulk changes in the ceramic powder grains were not observed nor expected below 1 GPa.

In part due to scaling, Nyquist plots can be inconvenient to discern phases (figure 2) as the semi circles, or time constants may differ in size by orders of magnitude. Imaginary modulus (M") was used as it can discern the grain boundary phase[15] as a local maxima (Figure 3), defined by equation 4.

$$M"_{max} = \frac{e_0}{2C_0} \quad (4)$$

$$\text{Also} \quad M"(\omega) = \frac{\varepsilon''}{\varepsilon'^2 + \varepsilon''^2} \quad (5)$$

In eq. 4 and 5, e_0 = 8,854pF/m - permittivity in vacuum , C_0= capacitance, and ε′/ ε′′ are real and imaginary permittivity (ε′is also known as dielectric constant, and ε′′ as dielectric loss). Due to the three dimensional nature of the materials, it was necessary to construct an equivalent circuit using parameters beyond this work, such as loss tangent, admittance, permittivity and so on with an exact match for this system found using the model in figure 4, with grain and grain boundaries labeled, the electrical contacts (E1 is the polished anvil/ceramic interface, and E2 is the non-polished steel shaft/ceramic interface) were also detectable using IS.

It is described by Behera *et al*[55] that a shift of M''_{max} to higher or lower frequency domain is a change in dielectric relaxation in agreement with Liu *et al*[56] (illustrated by example in figure 3, LAGP (as received) pressed from 0.00-0.75GPa) who also describe merging of peaks at higher temperatures due to the conduction process. Moreover, as we are attempting to characterize a material that relies on ion hopping for conductance, the usual methods are sometimes inadequate. Interestingly, the work of Ngai and León[57] strongly supports using electric modulus to characterize the conductance of ions through a disordered solid, and seem to strongly support our findings in this study. Bulk ion hopping defined by Barsoukov and MacDonald as the inverse of the frequency at $M"_{max}$ is the conductivity relaxation time, τ_σ. The relationship[57] can be described by equation 6, permittivity (dielectric) is defined in equation 7.

$$\frac{\tau_{ion}}{\tau_\sigma} = \frac{cq^2r^2}{6k_BT\varepsilon_0\varepsilon_\infty} \quad (6)$$

$$\varepsilon^* = M^{*-1} = \varepsilon' - j\varepsilon'' \quad (7)$$

(ε_∞= constant, and is the dielectric permittivity of the material, q is charge (1), k_B is the Boltzmann constant (8.854 * 10^{-12} F/m), c is concentration, T is temperature , and ε_0 all of which are constant) so $\tau_{ion} \propto r^2$, and τ_σ is determined by impedence spectra) Thus a shift in M''_{max} indicated a shift in τ_{ion} when r, the mean hopping distance of the ions , is the variable. Similar behavior is seen here, but at isothermal conditions. These frequency dependent changes indicate changes in relaxation times, and activation energies. Arrhenius plots may be calculated by equations 8 and 9

$$\tau_{peak} = \tau_0 \, Exp\,(\,{}^{Ea}/_{K_B T}) \quad (8)$$

$$\tau_{peak} = {}^{1}/_{2\pi f^{peak}} \quad (9)$$

Where τ_{peak} and f_{peak} are values at the local maxima on an F v. M" plot. A frequency shift of M" maxima will yield Arrhenius-like data plots using τ value. The decreasing size of the time constants in a Nyquist plot such as in figure 7 emulate the changes when subjected to increases in temperature (see supplemental information).

However literature to this point does not discern between τ_{ion} and τ_σ. The difference can be explained by changes in mean proximity of the grains or the reduced inter-grain hopping distance, which in turn would increase both ion hopping frequency and ratio of complete hops from one site to another resulting from this reduction in activation energy while other conditions remain constant.

2.4 X-ray diffraction studies

Initially samples were examined for crystal structure which matched well to the product diffractograms provided from the manufacturer (Figure 3a). Subsequent diffractograms were taken for treated heat and/or pressure treated samples for comparison, to ensure crystal changes were not occurring for samples of interest. With the exception of twice annealed LATP and LLT, no crystal changes were observed. These are discussed further in the supplemental information.

2.5 Annealing

Annealing temperatures were determined by literature, and by experimentation. The aim was to relieve surface stress and optimize the ceramics. Annealing was conducted in an argon tube furnace, and in air for comparison. Some samples were reversibly reduced in argon indicated by a change in

color, which was reversible by subsequent annealing in air. LATP when twice annealed in this fashion showed great improvement in conductivity. However, small crystal changes were observed, and were not investigated in this work. This is referred to hereafter as twice annealed LATP. Subsequent annealing in air resulted in LATP returning to a normal white color.

3. Results

3.1 IS pressure studies

In General, conductance increased for LAGP, LATP, and LLZO samples with increased pressure. We think that the intra-grain structure of the pressed sample collapses at some threshold pressure from mechanical failure, changing the system and thus the conductivity values. Unlike the other ceramics, LLTO samples decreased in conductance probably by affects described elsewhere[40] and LLT did not have a reproducible response.

Using IS, grain boundary impedance (Z_{GB}) is typically much larger by several orders of magnitude than the bulk impedance of the ceramic crystal (Z_B). In these results the signal for bulk impedance (grains) are overwhelmed by the grain boundary impedance signal. In the high frequency range, the boundary is short circuited and capacitively conducting and negligible in magnitude, while the lower frequency 2nd semicircle is in the time domain, and more closely resembles direct current in natures, mostly grain-to-grain conduction that varies with grain proximity[42].

As the pressure increases within the confined space grains are forced closer, and rearrangement for stability until some upper mechanical limit is reached resulting in fracture and collapse of grain arrangement. Samples respond differently, many reaching a threshold where conductance abruptly increases, while others decrease.

This mechanical breakage resulting in smaller grains, and changing surface area (SA) the distance between grains (l) is dynamic in this pressurized system. For disordered systems which consist mostly of capacitive grain boundaries characterized by Sakamaki et al[40], it is reasonable to modify the equation for capacitance to reflect changing conditions in this system (equation 6).

$$dC = e_0 \frac{\partial A}{\partial l} \quad or \quad dC = e_0 \left(\frac{\partial A}{\partial l}\right)_P \qquad (6)$$

C =capacitance, A surface area, l (grain boundary) length and P pressure.

The brick layer model is conceptually sound even in simple form, but has been updated[41-45] in literature to account for grain size, geometry, percent of grain contact and so on, leaving the door open to perhaps model such systems better in the future.

With a grain boundary conductance that is much lower than the bulk as it is here, admittance equations may characterize a system in part (equation 11) when $\sigma_b >> \sigma_{gb}$ or 12 where $\sigma_{gb} >> \sigma_g$. Ψ_t is total admittance, x is volume fraction, g is grain, gb grain boundary, for systems with known volumes of grain and grain boundaries. Pore space was measured using the Archimedes method, and it could possibly be used, in part, to determine the aforementioned volumes.

Sample pellets formed at maximum pressure (0.75 GPa typically) had a measured porosity between 18-30%, without the use of binders. While not elastic, some relaxation of pelletized ceramics was expected and observed when released from the sample holder, therefore voids and pore space are larger in a formed pellet than when subjected to pressure.

While it is easy to make the assumption that the grains get closer together and more compact, and that conduction may improve, the underlying mechanisms are quite complex and interesting. Application of pressure up to 1.0 GPa is not alone sufficient to cause a crystallographic change in the samples, so we can say that the changes in electrical measurements are a result of mechanical forces.

Twice annealed LATP conductance increased abruptly between 0.45 and 0.60 GPa (figure 7F). it is speculated that the inter-grain structure in the sample cylinder collapses above 0.45 GPa causing a settling of the LATP powder thus increasing surface contacts and reducing grain boundary regions. Example spectra LAGP as received M" vs. log F indicates a lateral peak shift, indicating a frequency dependency and change in relaxation time. Magnitude of peaks indicates change in capacitance (eq. 2) LLTO versus LLTO annealed shows a decrease in σ is observed for annealed samples. LLZO and LAGP likewise showed improved conductance under pressure, and with annealing. Additional ε′ and M′′vs. F trends are discussed in the supplementary information section.

3.2 Scanning electron microscopy (SEM)

Micrographs were taken at each experimental step when possible. Upon annealing, grains appear better defined. Calculations of average diameter indicate smaller average sizes for pressed, annealed, and annealed then pressed powders which were expected, likely due to mechanical stress and exploitation of surface cracks and imperfections by the heating process and/or pressure.

Consequently this changes the overall grain size distribution, therefore a resulting change in grain and grain boundary surface areas. Most notably for LATP, an abrupt change in grain boundary impedance was noted probably due to collapse in intra-grain structure which occurred at about 0.45GPa.

SEM images of samples illustrate what would be expected, that the grains are closer together with consolidation of grain boundaries which range are quite large, with voids for unconsolidated samples to closely packed grains for samples subjected to pressure to form pellets. Moreover some physical changes can be observed for the grains themselves for LAGP, LLZO and LATP. Visually the consistency of the ceramic powders differs from each treatment.

2.6 TGA Analysis

Powders as received were pressed into pellets to 0.75GPa prior to TGA analysis. All powders showed loss of weight due to increase of temperature, possibly due to retained water[60-62] , trapped gases[25], decomposition [63], or removal of synthesis residuals [62] . This alone could change the outcome for powders that were annealed then pressed compared to powders that were pressed, and then annealed because these contaminants could be reintroduced when pelletizing annealed powder.

Samples were ramped 10°C / min to annealing temperatures, held isothermally 60 minutes under nitrogen then cooled to 50°C (figure 9). At this step the flowing gas was switched (nitrogen, argon, or air) and held isothermally for 48 hours to observe weight changes summarized in Table 2. Improvement in conductance by gas replacement in the pores has been speculated elsewhere, and should not be ruled out. Breathing quality air[A] was used in place of oxygen. Samples were allowed to stand 48 hours after cooling to observe weight change. The decrease in weight suggests possible consolidation of grains and decreased pore space of pellets, as well as an indication of pore space availability in each pressed ceramic pellet.

Discussion

In all ceramic systems described, grain boundary impedance dominates each system. This results in a rather low ionic conductivity overall for a disordered powder system. This is mitigated somewhat by the process of compressing the powders into a pellet, and by annealing the powders. Other possible methods would be ball milling which would be a consideration when using commercially available powders if a more uniform system is not available for purchase.

Without sintering, changes were observed at the grain boundary regions utilizing a novel application of IS such as modulus which has been in use but not a great deal over the years Modulus

allows the observation of the grain boundary capacitance shift due to relaxation processes at the grain boundary[64] in ways that are not possible with other methods. Nyquist plots while valuable, tend to dominate battery research where impedance measurements are concerned. Here, we associate electrochemical measurements with physical changes in the system which strongly suggests a connection between grain boundary conditions, pressure, and impedance based values.

Changes in electric modulus indicate capacitance changes pertaining to available surface areas, and proximity which could correlate to hopping frequency and relaxation times of ions during the hopping process. Likewise, this focuses more on the grain boundary as the bulk ceramics have been well studied in literature, neglecting somewhat the underlying mechanisms present in disordered solids. Changes in permittivity under pressure are indicative of polarization suggests a qualitative change in how easily a sample becomes polarized, which essentially a charge transfer through a material. This supports the observed changes in ion conductivity, as positive ions are transferred through as sample; this is countered by movement of negative charge. Our results do not indicate specific frequency dependence for permittivity, rather a general trend.

Here we have characterized and compared the changes in conductivity and other electrical properties of five commercially available lithium conducting ceramics, the interactions at the grain boundaries, and attempting to resolve these changes under different pressurized conditions without effecting a structural change in the bulk. A better understanding of the mechanisms involved is a step forward in realizing the production of solid state batteries, their practical and reliable use.

Acknowledgments

The authors would like to acknowledge members of The University of Tulsa Nanotechnology Institute for support and useful discussion from its members. JWO would like to thank the University of Tulsa Graduate School and Office of Research for travel funding for promoting this work. The work was supported in part by the Oklahoma Center for the Advancement of Science and Technology (OCAST) and NASA Grant No. NNX13AN01A issued through the NASA EPSCoR Program.

References

1. Fergus, J. W., Ceramic and polymeric solid electrolytes for lithium-ion batteries. *Journal of Power Sources* **2010,** *195* (15), 4554-4569.
2. Kumar, J.; Kichambare, P.; Rai, A. K.; Bhattacharya, R.; Rodrigues, S.; Subramanyam, G., A high performance ceramic-polymer separator for lithium batteries. *Journal of Power Sources* **2016,** *301*, 194-198.
3. Thangadurai, V.; Weppner, W., Recent progress in solid oxide and lithium ion conducting electrolytes research. *Ionics* **2006,** *12* (1), 81-92.
4. Liu, W. Multilayer composite solid electrolytes for Lithium Ion Batteries. Ph.D., Syracuse University, 2016.
5. Knauth, P., Inorganic solid Li ion conductors: An overview. *Solid State Ionics* **2009,** *180* (14–16), 911-916.
6. Rangasamy, E.; Wolfenstine, J.; Allen, J.; Sakamoto, J., The effect of 24c-site (A) cation substitution on the tetragonal–cubic phase transition in Li7−xLa3−xAxZr2O12 garnet-based ceramic electrolyte. *Journal of Power Sources* **2013,** *230*, 261-266.
7. Murugan, R.; Thangadurai, V.; Weppner, W., Fast Lithium Ion Conduction in Garnet-Type Li7La3Zr2O12. *Angewandte Chemie International Edition* **2007,** *46* (41), 7778-7781.
8. Mariappan, C. R.; Gnanasekar, K. I.; Jayaraman, V.; Gnanasekaran, T., Lithium ion conduction in Li5La3Ta2O12 and Li7La3Ta2O13 garnet-type materials. *Journal of Electroceramics* **2013,** *30* (4), 258-265.
9. Murugan, R.; Thangadurai, V.; Weppner, W., Effect of lithium ion content on the lithium ion conductivity of the garnet-like structure Li5+xBaLa2Ta2O11.5+0.5x (x = 0–2). *Applied Physics A* **2008,** *91* (4), 615-620.
10. Kosova, N. V.; Devyatkina, E. T.; Stepanov, A. P.; Buzlukov, A. L., Lithium conductivity and lithium diffusion in NASICON-type Li1+xTi2–xAlx(PO4)3 (x= 0; 0.3) prepared by mechanical activation. *Ionics* **2008,** *14* (4), 303-311.
11. Thangadurai, V.; Weppner, W., Effect of B-site substitution of (Li,La)TiO3 perovskites by di-, tri-, tetra- and hexavalent metal ions on the lithium ion conductivity (E4). *Ionics* **2000,** *6* (1), 70-77.
12. Evgenij Barsoukov, J. R. M., Impedance Spectroscopy: Theory, Experiment, and applications 2nd edition. 2005 ed.; John Wiliey & Sons: 2005; p 581.
13. Murugan, R.; Thangadurai, V.; Weppner, W., Lithium ion conductivity of Li5+x Ba x La3−x Ta2O12 (x = 0–2) with garnet-related structure in dependence of the barium content. *Ionics* **2007,** *13* (4), 195-203.
14. Kothari, D. H.; Kanchan, D. K., Study of Li+ conduction in Li1.3Al0.3−xScxTi1.7(PO4)3 (x=0.01, 0.03, 0.05 and 0.07) NASICON ceramic compound. *Physica B: Condensed Matter* **2016,** *494*, 20-25.
15. Irvine, J. T. S.; Sinclair, D. C.; West, A. R., Electroceramics: Characterization by Impedance Spectroscopy. *Advanced Materials* **1990,** *2* (3), 132-138.
16. Hagman, L.-o. K., Peder, The Crystal Structure of $NaMe_s^{IV}(PO_4)_3$: Me^{IV} = Ge, Ti, Zr. *Acta Chemica Scandinavica* **1968,** *22*, 1822-1832.
17. Aono, H.; Sugimoto, E.; Sadaoka, Y.; Imanaka, N.; Adachi, G. y., Ionic Conductivity of the Lithium Titanium Phosphate (Li1 + X M X Ti2 − X (PO 4) 3 , M = Al , Sc , Y , and La) Systems. *Journal of The Electrochemical Society* **1989,** *136* (2), 590-591.
18. Li, S.-C.; Lin, Z.-X., Phase relationship and ionic conductivity of Li1+xTi2−xInxP3O12 system. *Solid State Ionics* **1983,** *9–10, Part 2*, 835-837.

19. Monchak, M.; Hupfer, T.; Senyshyn, A.; Boysen, H.; Chernyshov, D.; Hansen, T.; Schell, K. G.; Bucharsky, E. C.; Hoffmann, M. J.; Ehrenberg, H., Lithium Diffusion Pathway in Li1.3Al0.3Ti1.7(PO4)3 (LATP) Superionic Conductor. *Inorganic Chemistry* **2016,** *55* (6), 2941-2945.
20. Zhao, E.; Ma, F.; Guo, Y.; Jin, Y., Stable LATP/LAGP double-layer solid electrolyte prepared via a simple dry-pressing method for solid state lithium ion batteries. *RSC Advances* **2016,** *6* (95), 92579-92585.
21. Aono, H.; Sugimoto, E.; Sadaoka, Y., Electrical properties of sintered lithium titanium phosphate ceramics (Li1+xMxTi2-x (PO4)3, M3+ = Al3+, Sc3+, or Y3+). *Chem Lett* **1990,** *10*.
22. Zu-xiang, L.; Hui-jun, Y.; Shi-chun, L.; Shun-bao, T., Phase relationship and electrical conductivity of Li1+xTi2−xGaxP3O12 and Li1+2xTi2−xMgxP3O12 systems. *Solid State Ionics* **1986,** *18–19, Part 1*, 549-552.
23. Duluard, S.; Paillassa, A.; Puech, L.; Vinatier, P.; Turq, V.; Rozier, P.; Lenormand, P.; Taberna, P.-L.; Simon, P.; Ansart, F., Lithium conducting solid electrolyte Li1.3Al0.3Ti1.7(PO4)3 obtained via solution chemistry. *Journal of the European Ceramic Society* **2013,** *33* (6), 1145-1153.
24. Song, W.; Ji, X.; Wu, Z.; Zhu, Y.; Yang, Y.; Chen, J.; Jing, M.; Li, F.; Banks, C. E., First exploration of Na-ion migration pathways in the NASICON structure Na3V2(PO4)3. *Journal of Materials Chemistry A* **2014,** *2* (15), 5358-5362.
25. Kumar, B.; Kichambare, P.; Rodrigues, S.; Kumar, J.; Keil, R. G., Lisicon Glass-Ceramics Mediated Catalysis of Oxygen Reduction. *Electrochemical and Solid-State Letters* **2011,** *14* (6), A97-A99.
26. Berbano, S. S.; Guo, J.; Guo, H.; Lanagan, M. T.; Randall, C. A., Cold sintering process of Li1.5Al0.5Ge1.5(PO4)3 solid electrolyte. *Journal of the American Ceramic Society* **2017,** *100* (5), 2123-2135.
27. Kotobuki, M.; Suzuki, Y.; Munakata, H.; Kanamura, K.; Sato, Y.; Yamamoto, K.; Yoshida, T., Effect of sol composition on solid electrode/solid electrolyte interface for all-solid-state lithium ion battery. *Electrochimica Acta* **2011,** *56* (3), 1023-1029.
28. Aono, H.; Sugimoto, E.; Sadaoka, Y.; Imanaka, N.; Adachi, G. y., Ionic Conductivity of Solid Electrolytes Based on Lithium Titanium Phosphate. *Journal of The Electrochemical Society* **1990,** *137* (4), 1023-1027.
29. Düvel, A.; Kuhn, A.; Robben, L.; Wilkening, M.; Heitjans, P., Mechanosynthesis of Solid Electrolytes: Preparation, Characterization, and Li Ion Transport Properties of Garnet-Type Al-Doped Li7La3Zr2O12 Crystallizing with Cubic Symmetry. *The Journal of Physical Chemistry C* **2012,** *116* (29), 15192-15202.
30. Redhammer, G. J.; Rettenwander, D.; Pristat, S.; Dashjav, E.; Kumar, C. M. N.; Topa, D.; Tietz, F., A single crystal X-ray and powder neutron diffraction study on NASICON-type Li1+xAlxTi2−x(PO4)3 (0 ≤ x ≤ 0.5) crystals: Implications on ionic conductivity. *Solid State Sciences* **2016,** *60*, 99-107.
31. Kothari, D. H.; Kanchan, D. K., Effect of doping of trivalent cations Ga3+, Sc3+, Y3+ in Li1.3Al0.3Ti1.7 (PO4)3 (LATP) system on Li+ ion conductivity. *Physica B: Condensed Matter* **2016,** *501*, 90-94.
32. Aguesse, F.; Manalastas, W.; Buannic, L.; Del Amo, J. M. L.; Singh, G.; Llordés, A.; Kilner, J., Investigating the dendritic growth during full cell cycling of garnet electrolyte in direct contact with Li metal. *ACS Applied Materials and Interfaces* **2017,** *9* (4), 3808-3816.

33. van Den Broek, J.; Rupp, J. L. M.; Afyon, S., Boosting the electrochemical performance of Li-garnet based all-solid-state batteries with Li4Ti5O12 electrode: Routes to cheap and large scale ceramic processing. *Journal of Electroceramics* **2017**, 1-7.
34. Tsai, C.-L.; Roddatis, V.; Chandran, C. V.; Ma, Q.; Uhlenbruck, S.; Bram, M.; Heitjans, P.; Guillon, O., Li7La3Zr2O12 Interface Modification for Li Dendrite Prevention. *ACS Applied Materials & Interfaces* **2016,** *8* (16), 10617-10626.
35. El Shinawi, H.; Janek, J., Stabilization of cubic lithium-stuffed garnets of the type "Li7La3Zr2O12" by addition of gallium. *Journal of Power Sources* **2013,** *225*, 13-19.
36. Allen, J. L.; Wolfenstine, J.; Rangasamy, E.; Sakamoto, J., Effect of substitution (Ta, Al, Ga) on the conductivity of Li7La3Zr2O12. *Journal of Power Sources* **2012,** *206* (Supplement C), 315-319.
37. Inaguma, Y.; Liquan, C.; Itoh, M.; Nakamura, T.; Uchida, T.; Ikuta, H.; Wakihara, M., High ionic conductivity in lithium lanthanum titanate. *Solid State Communications* **1993,** *86* (10), 689-693.
38. Ahmad, M. M., Lithium ionic conduction and relaxation dynamics of spark plasma sintered Li5La3Ta2O12 garnet nanoceramics. *Nanoscale Research Letters* **2015,** *10* (1), 1-10.
39. Onishi, H.; Takai, S.; Yabutsuka, T.; Yao, T., Synthesis and Electrochemical properties of LATP-LLTO lithium ion conductive composites. *Electrochemistry* **2016,** *84* (12), 967-970.
40. Sakamaki, R.; Sakamoto, N.; Fujiki, H.; Kaneko, N. H., Local DC electrical properties of La2/3-xLi3xTiO3 grain boundaries. *Nippon Seramikkusu Kyokai Gakujutsu Ronbunshi/Journal of the Ceramic Society of Japan* **2016,** *124* (9), 907-910.
41. Maier, J., On the Conductivity of Polycrystalline Materials. *Berichte der Bunsengesellschaft für physikalische Chemie* **1986,** *90* (1), 26-33.
42. Fleig, J.; Maier, J., Finite-Element Calculations on the Impedance of Electroceramics with Highly Resistive Grain Boundaries: I, Laterally Inhomogeneous Grain Boundaries. *Journal of the American Ceramic Society* **1999,** *82* (12), 3485-3493.
43. Bouchet, R.; Knauth, P.; Laugier, J.-M., Theoretical analysis of the impedance spectra of electroceramics Part 2: isotropic grain boundaries. *Journal of Electroceramics* **2006,** *16* (3), 229-238.
44. Kidner, N. J.; Perry, N. H.; Mason, T. O.; Garboczi, E. J., The Brick Layer Model Revisited: Introducing the Nano-Grain Composite Model. *Journal of the American Ceramic Society* **2008,** *91* (6), 1733-1746.
45. Erdoğan, S. T., Simple Estimation of the Surface Area of Irregular 3D Particles. *Journal of Materials in Civil Engineering* **2016,** *28* (8), 04016062.
46. Inaguma, Y.; Nakashima, M., A rechargeable lithium–air battery using a lithium ion-conducting lanthanum lithium titanate ceramics as an electrolyte separator. *Journal of Power Sources* **2013,** *228*, 250-255.
47. Kalnaus, S.; Tenhaeff, W. E.; Sakamoto, J.; Sabau, A. S.; Daniel, C.; Dudney, N. J., Analysis of composite electrolytes with sintered reinforcement structure for energy storage applications. *Journal of Power Sources* **2013,** *241*, 178-185.
48. Hiratani, M.; Miyauchi, K.; Kudo, T., Electrode reaction at the interface between a lithium anode and a solid electrolyte. *Solid State Ionics* **1988,** *28-30*, 1431-1435.
49. Jackman, S. D.; Cutler, R. A., Effect of microcracking on ionic conductivity in LATP. *Journal of Power Sources* **2012,** *218*, 65-72.

50. Schell, K. G.; Bucharsky, E. C.; Lemke, F.; Hoffmann, M. J., Effect of calcination conditions on lithium conductivity in Li1.3Ti1.7Al0.3(PO4)3 prepared by sol-gel route. *Ionics* **2016**, 1-7.
51. Tian, F.; Ohki, Y., Electric modulus powerful tool for analyzing dielectric behavior. *IEEE Transactions on Dielectrics and Electrical Insulation* **2014,** *21* (3), 929-931.
52. Vasoya, N. H.; Jha, P. K.; Saija, K. G.; Dolia, S. N.; Zankat, K. B.; Modi, K. B., Electric Modulus, Scaling and Modeling of Dielectric Properties for Mn2+-Si4+ Co-substituted Mn-Zn Ferrites. *Journal of Electronic Materials* **2016,** *45* (2), 917-927.
53. Fuqiang Tian; Ohki, Y., Electric Modulus a Powerful Tool for Analyzing Dielectric Behavior. *IEEE Transactions on Dielectrics and Electrical Insulation* **2014,** *21* (3), 1433-1433.
54. Belal Hossen, M.; Akther Hossain, A. K. M., Complex impedance and electric modulus studies of magnetic ceramic Ni0.27Cu0.10Zn0.63Fe2O4. *Journal of Advanced Ceramics* **2015,** *4* (3), 217-225.
55. Behera, A. K.; Mohanty, N. K.; Satpathy, S. K.; Behera, B.; Nayak, P., Investigation of complex impedance and modulus properties of Nd doped 0.5BiFeO3-0.5PbTiO3 multiferroic Composites. *Central European Journal of Physics* **2014,** *12* (12), 851-861.
56. Liu, J.; Duan, C.-G.; Yin, W.-G.; Mei, W. N.; Smith, R. W.; Hardy, J. R., Dielectric permittivity and electric modulus in Bi2Ti4O11. *The Journal of Chemical Physics* **2003,** *119* (5), 2812-2819.
57. Ngai, K. L.; León, C., Relating macroscopic electrical relaxation to microscopic movements of the ions in ionically conducting materials by theory and experiment. *Physical Review B* **1999,** *60* (13), 9396-9405.
58. Wang, Y. H., Kun; Zu, Chengkui; Chen, Jiang, Study on crystallization kinetics of Li2)-Al2O3-TiO2-P2O5 glass by non-isothermal techniques. *Advanced Materials Research* **2012,** *535-537*, 1629-1633.
59. Jeff Wolfenstinea, E. R., Jan L. Allen, Jeffrey Sakamoto, High conductivity of dense tetragonal Li7La3Zr2O12. *Journal of Power Sources* **(2012),** *208*, 193–196.
60. Mazumdar, D.; Bose, D. N.; Mukherjee, L. L.; Basu, A.; Bose, M., 7Li NMR and related studies in LISICON system. *Materials Research Bulletin* **1983,** *18* (1), 79-86.
61. Waetzig, K.; Rost, A.; Langklotz, U.; Matthey, B.; Schilm, J., An explanation of the microcrack formation in Li1.3Al0.3Ti1.7(PO4)3 ceramics. *Journal of the European Ceramic Society* **2016,** *36* (8), 1995-2001.
62. Belam, W., Sol–gel chemistry synthesis and DTA–TGA, XRPD, SIC and 7Li, 31P, 29Si MAS–NMR studies on the Li-NASICON Li3Zr2−ySi2−4yP1+4yO12 ($0 \leqslant y \leqslant 0.5$) system. *Journal of Alloys and Compounds* **2013,** *551*, 267-273.
63. Zangina, T.; Hassan, J.; Matori, K. A.; Azis, R. a. S.; Ahmadu, U.; See, A., Sintering behavior, ac conductivity and dielectric relaxation of Li1.3Ti1.7Al0.3(PO4)3 NASICON compound. *Results in Physics* **2016,** *6*, 719-725.
64. Feliciangeli, M. C.; Rossi, M. C.; Conte, G., An admittance spectroscopy study of grain and grain boundary of diamond. *Diamond and Related Materials* **2007,** *16* (4), 930-934.

Figures

Figure 1

The steel shaft is inserted into the tube, and O-rings were used on both shaft and tube to facilitate vacuum

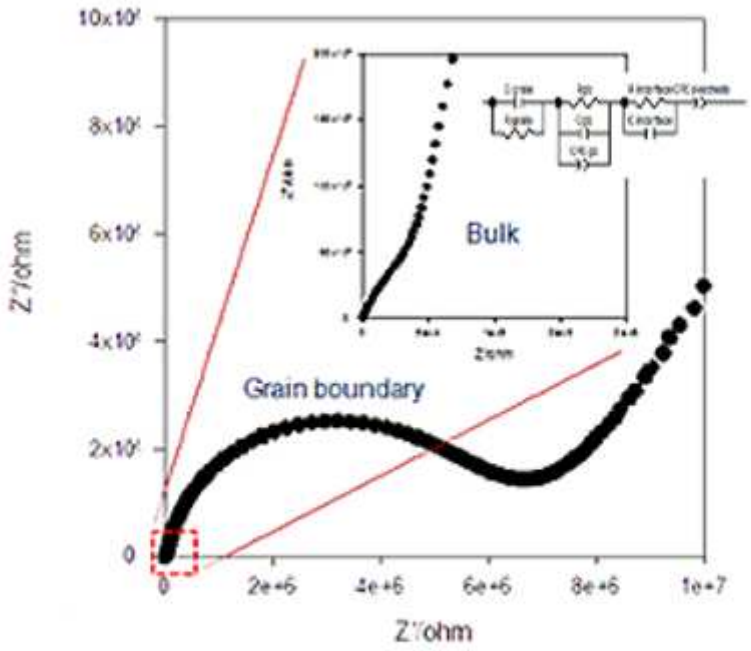

Figure **2**

Figure 2

In part due to scaling, Nyquist plots can be inconvenient to discern phases as the semi circles

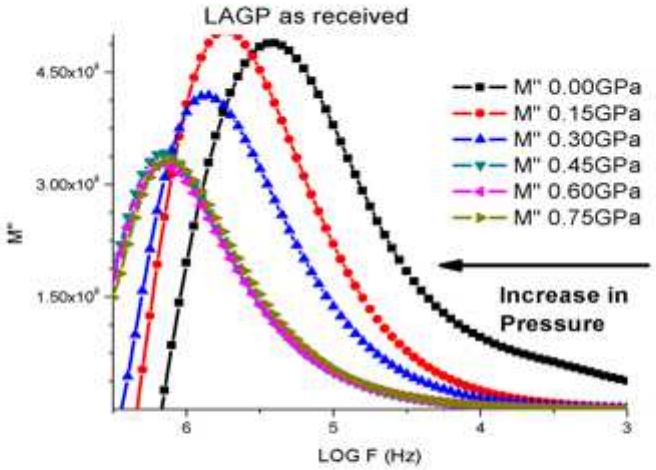

Figure **3**

Figure 3

LAGP (as received) pressed from 0.00-0.75GPa)

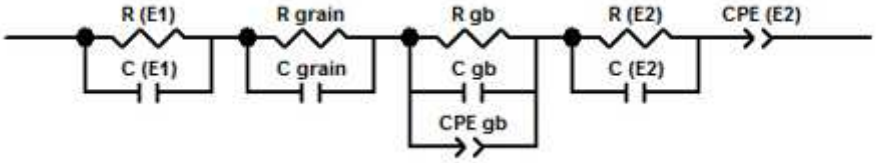

Figure 4

equivalent circuit model

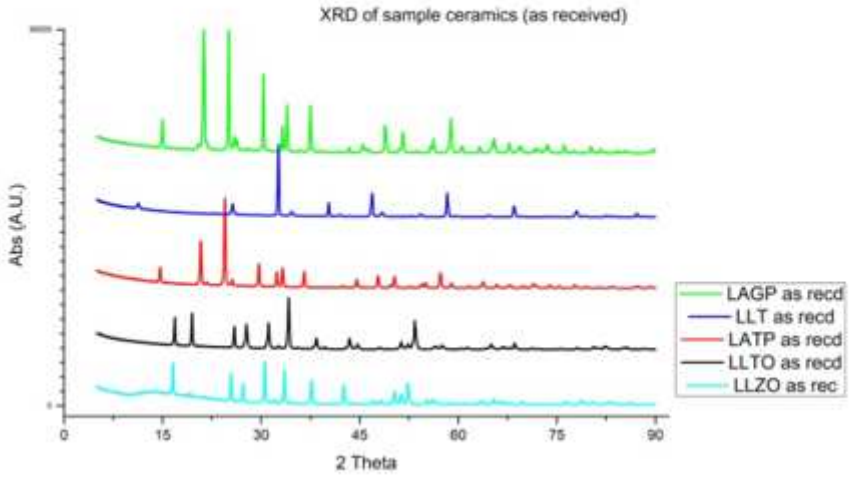

Figure 5

comparison of ceramic powers used

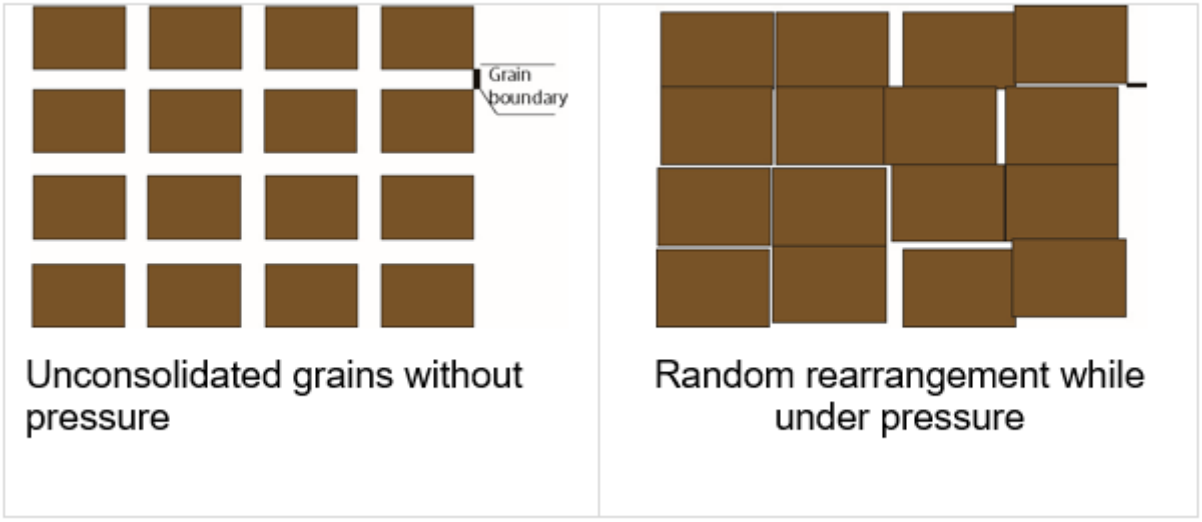

Figure 6

simplified brick and mortar model

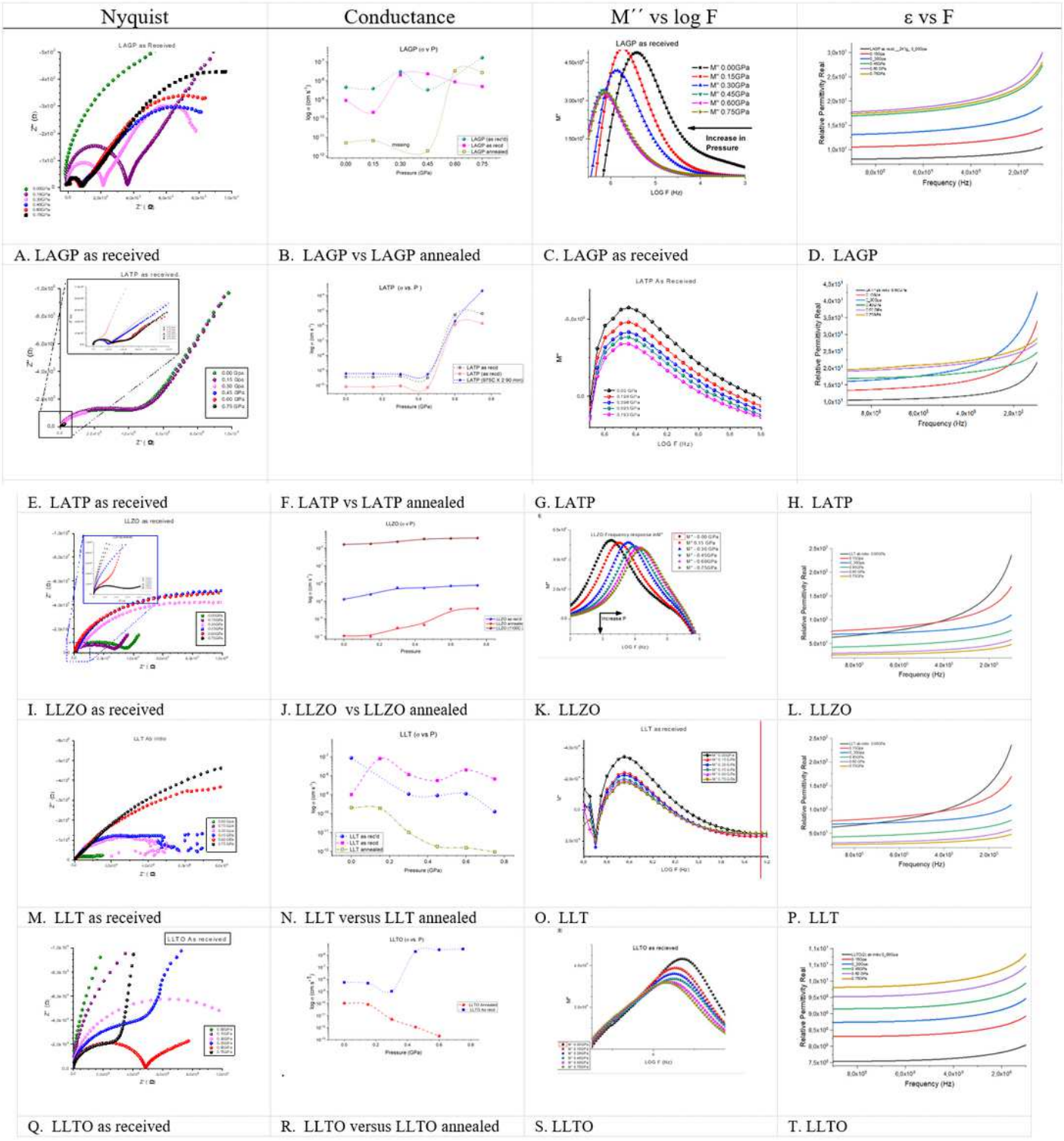

Figure 7

from left to right for samples as received (exept conductance plot): Nyquist plot, sample counductance under pressure, electric modulus changes under pressure, and permittivity changes under pressure for

each labeled ceramic.

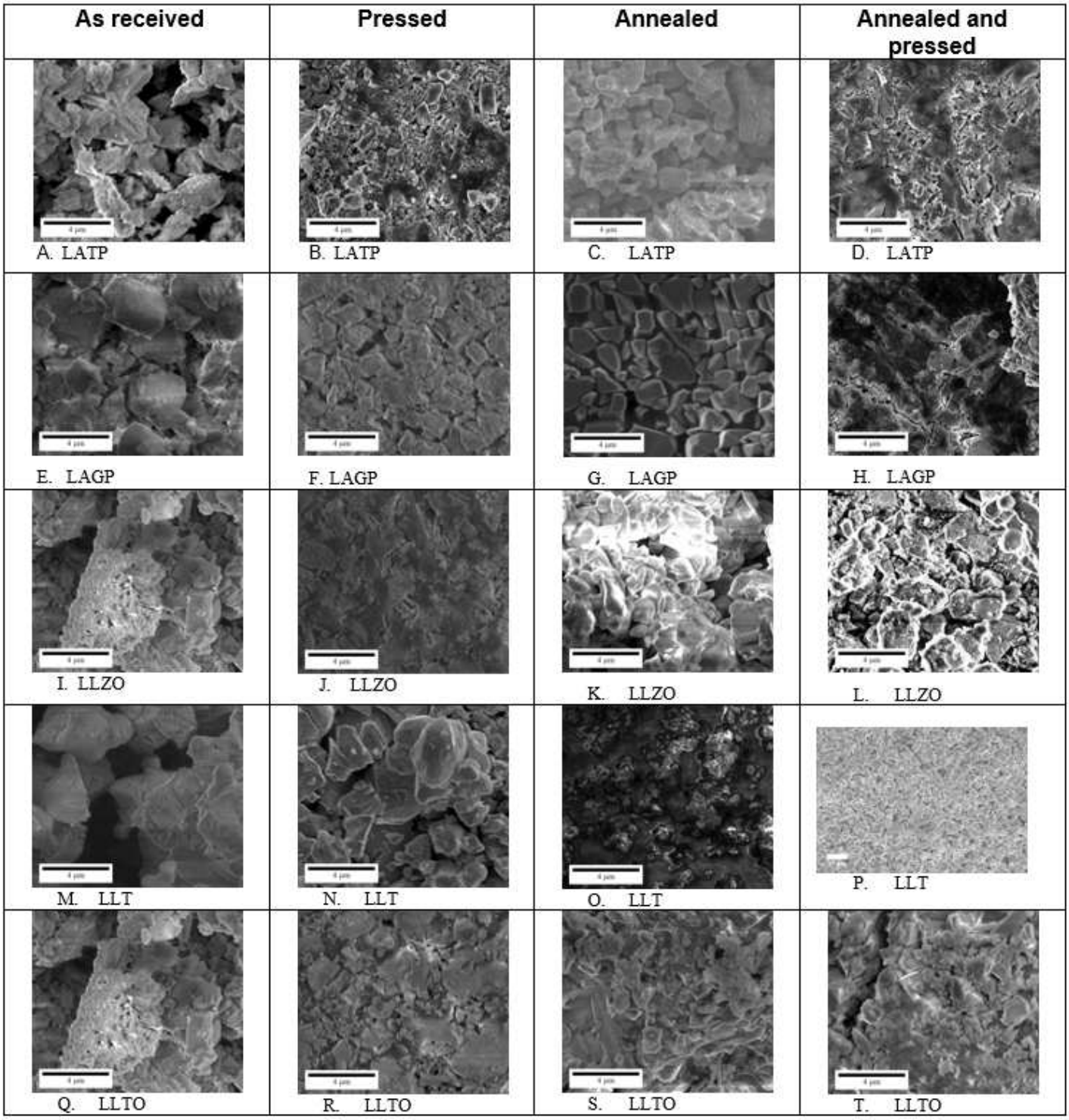

Figure 8

SEM for each ceramic tested from left to right: as received, pressed, annealed (not pressed), and annealed and pressed.

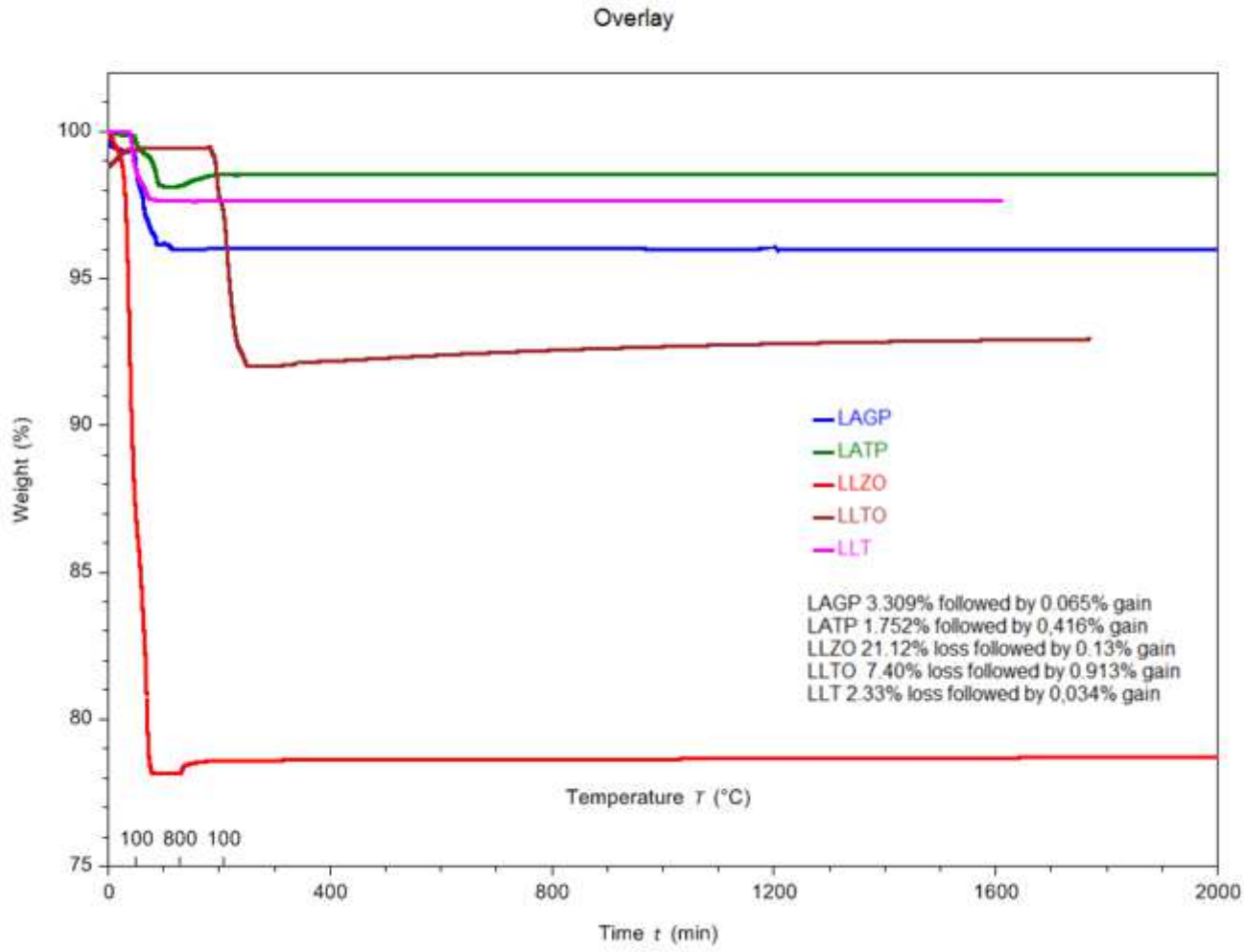

Figure 9

select TGA values for ceramic pellets

Supplementary Files

This is a list of supplementary files associated with this preprint. Click to download.

- Tables.pdf
- CeramicsSupplementaryinfoJWOFInal.docx